Revealing the inherent susceptibility of pathogenic bacteria to magnetic hyperthermia

Swati Kaushik[1], Jijo Thomas[1], Vineeta Panwar[1], Preethi Murugesan[1], Vianni Chopra[1], Navita Salaria[1], Rupali Singh[1], Himadri Shekar Roy[1], Rajesh Kumar[2], Vikas Gautam[2], Deepa Ghosh[1*]

[1] Chemical Biology Unit, Institute of Nano Science and Technology, Knowledge City, Sector 81, Mohali, Punjab 140306, India

[2] Post Graduate Institute of Medical Education & Research (PGIMER), Chandigarh, India

*Corresponding author: Deepa.ghosh@inst.ac.in

Research Highlights

- Pathogenic bacteria in presence of both Fe and zinc, form intracellular magnetic nanoparticles (MNP).
- The MNP conferred bacteria with magnetic field responsive movement and magnetic field-induced hyperthermia.
- Virulent bacteria acquire these elements from the host and form MNP.
- Exposure of infected tissues to alternating magnetic field results in significant reduction in bacterial load.

Abstract

One of the greatest challenges in healthcare is the increasing incidence of antibiotic resistance that appear to outpace the development of new antibiotics. Therefore, there is an urgent need to develop alternate strategies to combat such bacterial infections. Elements like iron and zinc are essential for the survival of bacteria. We evaluated the response of bacteria to these elements, using $FeCl_2$ and zinc gluconate as precursors. The bacteria treated with the combination of Fe and Zn showed intracellular magnetic nanoparticles (MNP) formation within 24-48 h and

exhibited magnetic field-induced magnetotaxis. Extensive characterization of the bacteria revealed intracellular presence of superparamagnetic zinc ferrite ($ZnFe_2O_4$) nanoparticles in the size range of 13-19 nm. On exposure of the treated bacteria to an alternating magnetic field, a significant temperature rise was observed which resulted in a drastic reduction in bacterial viability. Using a similar approach, biofilms showed a comparable reduction in bacterial viability. Given the ability of virulent bacteria to acquire these elements from the body, evaluation of virulent bacteria obtained from infected human tissues revealed the presence of intracellular MNP, and their susceptibility to magnetic hyperthermia. The results suggested that the proposed strategy can evolve as an antibiotic-free approach to treat infectious bacteria, including antibiotics-resistant bacteria.

Graphical Abstract

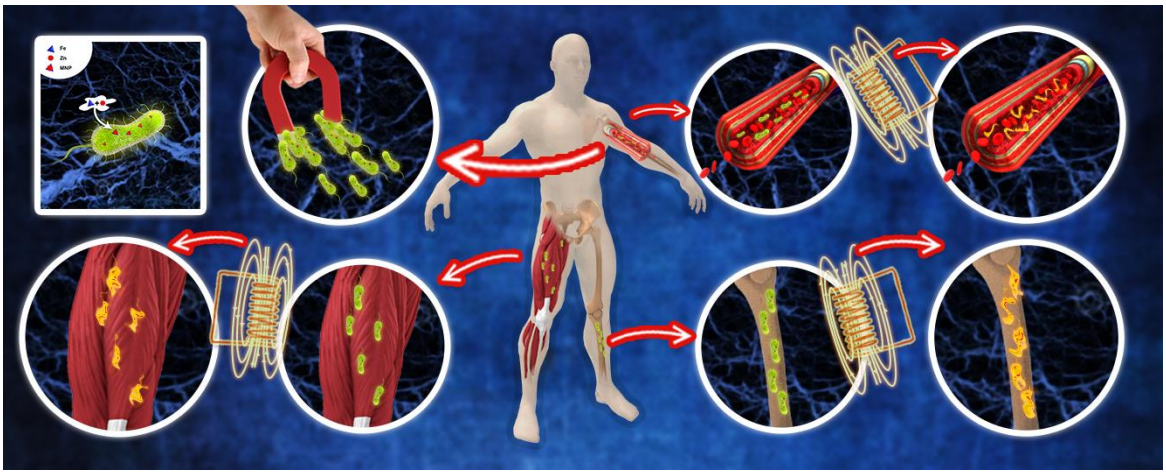

Pathogenic bacteria form intracellular magnetic nanoparticles (MNP) in presence of iron and zinc elements. The MNP endow the bacteria, magnetic-filed responsive migration and susceptibility to magnetic hyperthermia

Keywords: Magnetic nanoparticles; Hyperthermia, Antibiotics, Biofilms, Magnetotaxis

Introduction

Ever since Alexander Fleming's discovery of Penicillin around eight decades ago, antibiotics have revolutionized the treatment of infections [1]. However, the growing incidence of bacterial resistance attributed to inappropriate antibiotics use in health-care, agriculture and veterinary

sectors is threatening to take us back to the pre-antibiotics era [2, 3]. With a decline in the discovery of new drugs that can handle the rising infections, the demand for the development of alternate strategies to avoid a possible health-care disaster is on the rise [4]. To obtain the best outcome, the strategy should be simple, cost effective and safe for humans, and efficacious against a wide range of Gram-positive and Gram-negative bacteria [5]. Magnetic nanoparticles (MNP) are used extensively in various fields like health care, biotechnology, environmental and material science for applications like bio-separation, bio-sensors, imaging (as contrast agent in MRI), therapeutics (magnetic hyperthermia in cancers), catalysis, information storage, electronics etc. as they exhibit unique properties such as superparamagnetism [6]. Ascribing to their magnetic property, MNPs are used for bacterial detection [7- 9], separation [10], imaging [11] and anti-bacterial activity [12, 13]. In all such applications, the synthesized MNP was further modified to prevent aggregation, improve solubility, safety and target the microbes.

The process of heating diseased tissue to an elevated temperature for a limited time is termed hyperthermia and is considered a promising treatment option for cancer and other diseases. Pathogenic bacteria are also reported to be susceptible to hyperthermia [14, 15]. MNPs are considered as good hyperthermia agents, as they absorb electromagnetic radiation when exposed to alternating magnetic field (AMF) of high frequency and subsequently convert it to localized heat. A major challenge in using MNP is of targeting the infectious bacteria, apart from MNP toxicity in the body when used in large scale [16] Despite antibody-functionalized MNP being used to recognize target species, they are short-lived and expensive [17]. As the magnetic properties of MNP are strongly dependent on multiple factors like size, shape etc., controlling these parameters is a challenge [18]. Additionally, the process is energy intensive and often yields aggregated particles with poor solubility [19]. In contrast to synthetic methods, biosynthesized nanoparticles have a narrow size range and are monodisperse [20].

Iron and zinc are essential elements for virtually all organisms. Whereas several studies have compared the influence of either Fe / Zn on microbes, no study has yet shown their combined effect. Recently we had observed MNP formation in eukaryotic cells exposed to ferrous chloride and zinc gluconate [21]. Given the importance of iron and zinc to bacteria, the study was extended to bacteria. All the treated microbes biosynthesized intracellular MNP within 24-48 h and exhibited magnetic field-induced migration. Characterization studies showed the MNP to be made of zinc ferrites. Superparamagnetic nature of the MNP was confirmed using Superconducting

Quantum Interference Device (SQUID). A magnetic field dependent temperature rise resulted in a drastic reduction of bacterial viability. Following the same approach, the bacteria in biofilms were similarly affected.

As part of the host defense system, bacterial access to elements such as iron and zinc is restricted by the host through a process termed nutritional immunity [22]. To facilitate their survival and replication, infectious bacteria overcome these hurdles by developing smart strategies to mine these metals from multiple host resources [23]. To ensure the acquired intracellular iron/zinc is maintained in its non-toxic form, bacteria have evolved highly sophisticated systems to balance the efflux/influx of these ions through multiple transport/scavenging/storage systems [24, 25].Apart from the above systems, we envisaged that the virulent bacteria in the host may also synthesize MNP. Evaluation of bacteria present in multiple infected tissues revealed intracellular evidence of MNP. A time-dependent temperature rise was observed in the samples exposed to AMF. Magnetic hyperthermia-induced cell death was observed in several samples, demonstrating the feasibility of regulating bacterial infections with magnetic hyperthermia.

Materials and Methods

Materials

LB media, zinc gluconate (TCI chemicals (India) Pvt. Ltd.), ferrous chloride (Sigma-Aldrich) were procured from the respective commercial sources. *Staphylococcus aureus*-ATCC 25923; *Escherichia coli*-ATCC 20922*; Pseudomonas aeruginosa*-ATCC 27853 *and Klebsiella pneumoniae*-ATCC 700603 were purchased from ATCC, USA.

Bacterial culture with $FeCl_2$ and zinc gluconate

A single colony from each plate of the respective Gram- positive and Gram-negative bacteria was grown in a suspension culture for 2 h in 5 mL of LB. This was transferred to 200 mL of fresh LB medium and grown until OD_{550}= 0.5-0.6 (~5-6 h). For treatment, sterilized salt solutions of $FeCl_2$ and zinc gluconate were added to the culture. The resulting suspension was incubated at 37°C with shaking at 180 rpm. At the end of treatment (24-48 h), the bacterial cultures were centrifuged at 1000 x *g*, at 4ºC and gently fixed for further analysis. To determine viability, the respective bacterial cultures after 48 h treatment were plated on agar plates to check for growth.

Perl's Prussian blue Staining

Bacterial cells treated with $FeCl_2$ and/or zinc gluconate for 36 h were pelleted and fixed on slides using 4% para-formaldehyde (PFA). The slides were incubated in a solution containing equal parts

of 2% hydrochloric acid and 2% potassium ferrocyanide for 20 min. The slides were then rinsed thrice with distilled water and dehydrated using graded alcohol. The slides were then mounted with DPX and visualized under microscope.

Magnetotaxis Study

To check the influence of magnetic field on bacterial culture, a drop of the individually treated bacteria was placed on a slide and a neodymium bar magnet was placed on the microscope stage near the drop, with the axis of the magnet parallel to the plane of the slide. The movie of the migration of the microbes towards the magnet was recorded at 15 X speed and 40X magnification under bright field (OLYMPUS, DC73).

Characterization:

For TEM analysis, the respective bacterial cells were fixed with 4% formaldehyde solution and drop casted on TEM grids. The grids were negatively stained using Uranyl acetate (.05%), washed and air dried. TEM analysis was carried out at 120 KV (JEOL JEM 2100 transmission electron microscope). For further characterization of nanoparticles the bacterial lysate was used. Nanoparticle size, EDAX, elemental mapping was evaluated using TEM. HR-TEM, SAED pattern and inter planar spacing was used to identify the composition of the nanoparticles. The crystalline structure of nanoparticle was determined by Bruker D8 Advanced X-ray diffraction (XRD) system, using Cu-Ka radiation source from 20 to 80 (2h) with an increment of 0.02 min^{-1} with the respective microbes after calcination at 300 ^{0}C. Fourier transform infrared (FT-IR) of lyophilized samples of the treated bacterial culture was recorded by ATR using VERTEX 70 FT-IR (Bruker) from 4000-400 cm^{-1} at 4cm^{-1} resolution. Quantitative estimation of iron and zinc in the bacterial cells (normalized to the number of cells/well) was done using ICP-MS (Agilent Technologies 7700 Series). Magnetic measurements to determine the magnetic properties of the nanoparticles and measurements of temperature dependence of magnetization (ZFC-FC curves) were conducted using a SQUID (Superconducting Quantum Interference Device) magnetometer.

ROS determination using carboxy-H_2DCFDA

Treated as well as untreated bacterial cells of *S. aureus* and *E. coli were* washed with phosphate-buffered saline (PBS) and treated with Carboxy-H_2DCFDA dye at a final concentration of 50 µg/ml in PBS. The cultures were incubated in dark for 30 minutes. For positive control, H_2O_2 (200µM) was used. ROS levels were assessed by the detection of green fluorescence

(excitation filter =482 ± 35 nm) using fluorescence plate reader. All DCFDA fluorescence intensities were calculated relative to H_2O_2 control.

Magnetic-field induced hyperthermia

The efficiency of the biosynthesized magnetic nanoparticles to induce hyperthermia was tested using the D5 heating system (nB nanoscale Biomagnetics, Zaragoza, Spain). Post-treated *E.coli* and *S.aureus* were placed in DM2 system and subjected to an alternating current (AC) magnetic field (H) f=164, 347 kHz with field amplitude of 400 Oe to determine the rise in temperature with a constant target-temperature program feedback at 43ºC set point for 30 min. A fluoro-optic thermometer fiber probe was used to probe the temperature every 0.2 s after switching on the magnetic field. The rise in temperature (Δt) was noted. The experiments were run in triplicates and each run time was set to 30 min. In order to calculate the reduction in cell viability the bacterial suspension post-AMF treatment was plated on LB agar plates (dilution factor 10^4). After 24 h of incubation, the colonies were counted and expressed as the number of cells versus AMF treatment. In case of infected human blood sample, the plasma was subjected to an alternating current (AC) magnetic field (H) f=347 kHz with field amplitude of 400 Oe to determine the rise in temperature for 30 min. Tissue and bone samples were subjected to an alternating current (AC) magnetic field (H) f=405 kHz with field amplitude of 400 Oe post homogenization. The experiments were run in triplicates and each run time was set to 30 min. In order to calculate the reduction in cell viability the plasma and homogenized tissue and bone samples post-AMF treatment were plated on LB agar plates (dilution factor 10^4). Following 24 h of incubation, the colonies were counted and expressed as the number of cells versus AMF treatment.

Effect on Biofilms

S.aureus and *E.coli* cells were cultured till they reached an OD_{600} of 0.6 was obtained, which corresponds to $3x10^8$ cells/ml. A dilution in nutrient media was made and 1ml of cell suspension was plated on glass coverslips and incubated at 37°C for 72 h. After 4 d of incubation a layer of biofilm was visualized. To the biofilms, Fe and Zn solution was added and further incubated for 36 h. Cells were subjected to hyperthermia at 405 KHz, 400 Oe for 30 min. In order to check the response of AMF treatment on cells, biofilms were subjected to live/dead staining after incubation with 5 µl (5 mg/ml) stock of FDA (Fluorescein diacetate, used for staining live cells green) and 2.5 µl (2 mg/ml) of PI (propidium iodide/used for damaged cells red) and visualized using Olympus microscope (OLYMPUS, DC73).

Statistical Analysis

Each statistical data is derived from a sample size of three, and the data is presented as mean ± standard deviation (SD). Graph Pad Prism 6 was used to analyze data and declared statistically significant if $P \leq 0.05$ as determined by one-way or two-way ANOVA test keeping a 95% confidence interval.

Results and Discussion

In this study, we evaluated the response of pathogenic strains of bacteria like *Staphylococcus aureus, Escherichia coli, Pseudomonas aeruginosa, and Klebsiella pneumoniae* to broth containing 1mM of $FeCl_2$ and zinc gluconate respectively for 24-48 h. A faint time-dependent darkening of broth was visible in the treated bacterial cultures (Fig S1). Microscopic evaluation of these cultures revealed microbial aggregation, in comparison to untreated control (Fig 1). On exposure to a magnetic field, the microbes grown in presence of iron and zinc exhibited magnetotaxis (Video S2-S9). To confirm whether the magnetic response is facilitated by intracellular iron oxide, we performed Perl's Prussian blue staining. A blue color noted in bacteria treated with Fe and Zn, confirmed the presence of iron oxide and revealed the importance of zinc in the intracellular iron uptake (Fig. 1) Fe and Zn content in the respective bacteria was estimated using IC-PMS (Table S1). A higher iron content observed only in those microbes treated with both iron and zinc, corroborated the results of Prussian blue studies (Fig 1).

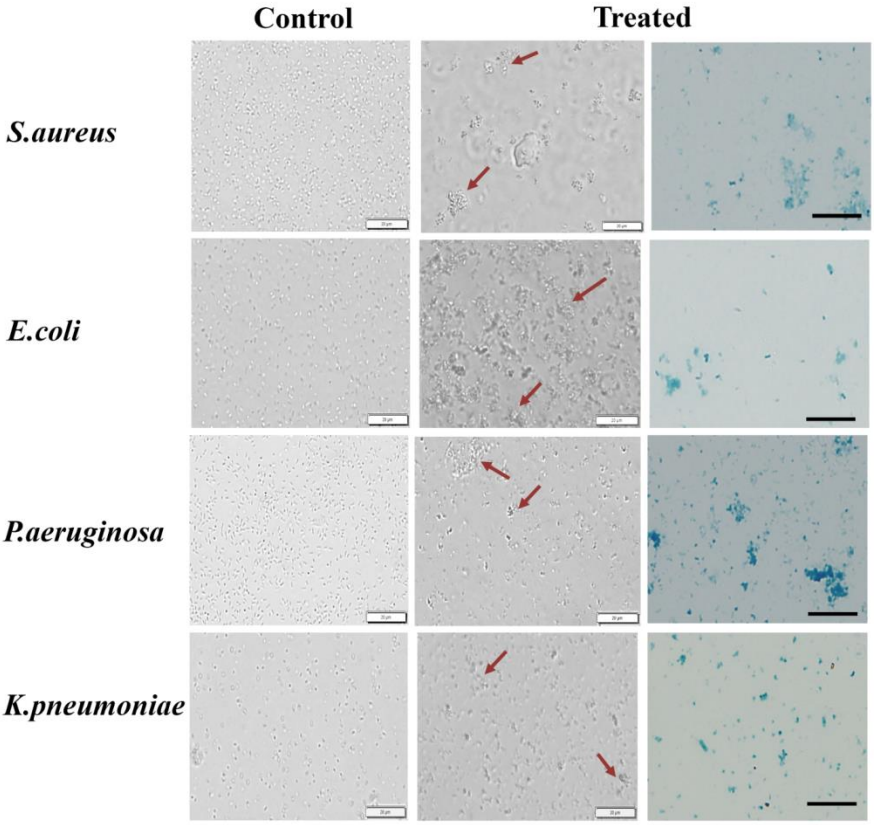

Fig. 1: Bacterial response to Fe and Zn. Bright field images of untreated (Left column) and treated bacteria (middle column). Arrows show bacterial aggregates. $FeCl_2$ and zinc gluconate treated bacteria stained with Perl's Prussian blue (Right column); Scale bar represents 20 μM.

The Gram-positive (S. *aureus*) and a representative Gram-negative bacterium (*E. coli*) were taken up for further characterization studies. TEM analysis of $FeCl_2$ and zinc gluconate treated *S. aureus* and *E. coli* revealed the presence of a large number of nanocrystals distributed throughout the respective bacteria (Fig 2 B, F), while no such crystals were observed in untreated control (Fig 2 A, E). On further analysis of the treated bacterial lysates, Quasi-cuboidal shaped particles (Fig 2I) of 13-19 nm size were observed (Fig 2J) [26]. HR-TEM images of individual nanocrystals clearly showed the lattice fringes, indicating the crystalline nature of the material [27]. The inter-planar spacing calculated from these fringes exhibited d-spacing of 0.283 nm and 0.489 nm corresponding to 100 planes of ZnO and 111 planes of zinc ferrite (ZnFe2O4) respectively (Fig 1C, G) [26, 28]. The diffraction spots indexed from selected area electron diffraction pattern (SAED) confirmed its crystalline nature having (111), (311), (220), (400), (511), (440) planes of $ZnFe_2O_4$ and (100),

(101), (110) plane of ZnO (Fig. 2 D, H) [29]. EDAX analysis (Fig 2K) and elemental mapping (Fig S11) confirmed the presence of iron, zinc and oxygen with homogeneous distribution of the above-mentioned elements.

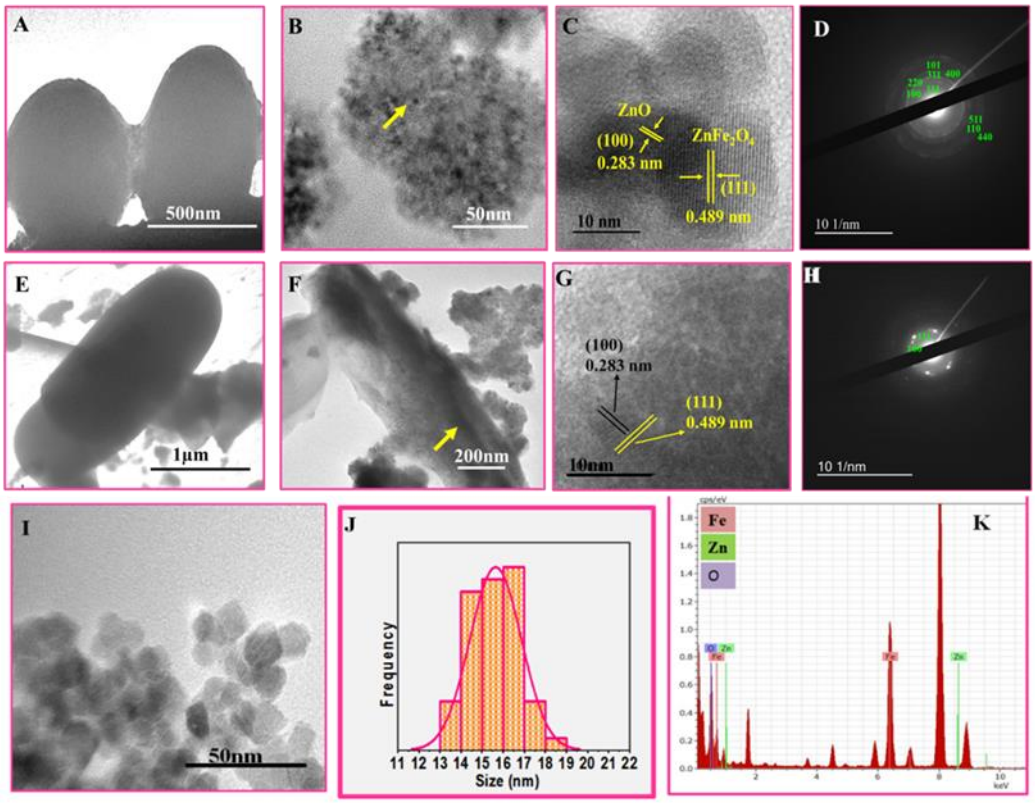

Fig 2: **Characterization of nanoparticles.** The upper and lower panel show TEM images of *S. aureus* and *E. coli* respectively. (A, E) Untreated bacteria; (B, F) Bacteria treated with $FeCl_2$ and zinc gluconate (arrow indicates nanoparticles); (C, G) HR-TEM showing D-Planar spacing of nanoparticles; (D, H) SAED pattern of nanoparticles; (I) TEM image of nanoparticles; (J) Size distribution of the nanoparticles (K) EDAX showing the presence of Fe, Zn and O obtained from *S. aureus*.

To evaluate the magnetic properties of the nanoparticles, field dependent magnetization measurements were performed on lyophilized samples of treated bacteria using SQUID. Fig 3 displays the magnetic properties (M-H loop at 300K (A), at 5K (B) and M-T curve (C) with *S. aureus*. At room temperature (300K), negligible coercivity was observed signifying the superparamagnetic behavior of the nanoparticles due to zero coercivity (inset, Fig 3A). The magnetic signal observed at 5 K displayed low coercivity (150 Oe: inset Fig 3B), confirming the

characteristic properties of superparamagnetism [30]. The zero field cooled (ZFC) and field cooled (FC) curves of the samples obtained at an applied field of 500 Oe further confirmed the superparamagnetic behavior with blocking temperature at ~ 150 K (Fig. 3C). A similar observation was observed with *E. coli* (Fig S12). As the superparamagnetism characteristics are generally exhibited by MNPs that exist as single domain particles, it can be concluded that the magnetic particles present in the treated bacteria are also single-domain superparamagnetic nanoparticles [31]. Additionally, zinc ferrite nanoparticles are reported to have better magnetization properties than iron oxide nanoparticles, which could be responsible for the observed magnetotaxis [32].

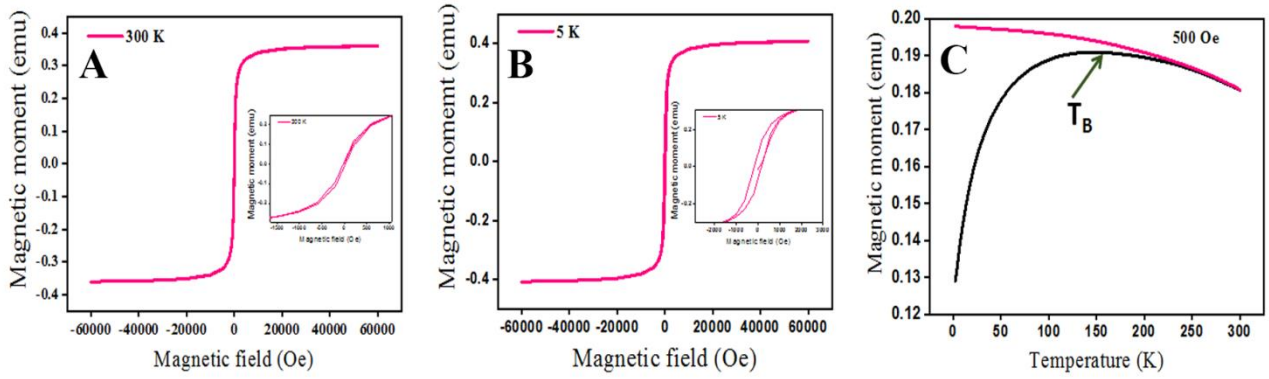

Fig 3: Magnetic measurement of nanoparticles in *S. aureus*. $FeCl_2$ and zinc gluconate treated bacteria were lyophilized and magnetization versus magnetic field was measured at (A) 300 K, (B) 5K and inset represents coercivity (C) Measurement of Temperature Dependence of Magnetization (FC/ZFC curves).

Further characterization of the treated bacteria using XRD revealed the crystalline nature of the *in situ* formed material (Fig S13A). The numerous strong Bragg reflections could be indexed to the presence of both ZnO and zinc ferrite phases [28] respectively, supporting the TEM results. The crystalline peaks at $2\theta = 31.73^o$, 36.2^o and 56.6^o represents (100), (101), (110) hkl plane correspond to the hexagonal crystal structure of ZnO according to JCPDS no. 36-1451 [33]. The peaks at $2\theta = 18.3^o$, 30.1^o, 35.2^o, 43.1^o, 53.3^o, 56.7^o and 62.4^o with hkl plane of (111), (220), (311), (400), (422), (511) and (440) correspond to the cubic spinel structure of $ZnFe_2O_4$ according to JCPDS no.79-1150 [29]. Fourier transform infrared (FTIR) analysis of the treated bacteria post its lyophilization also exhibited peaks in the region from 670-550 cm^{-1} reflecting the stretching vibration mode associated to Fe–O bonds in the crystalline lattice of $ZnFe_2O_4$ [27]. The other peaks observed in the region from 476-417 cm^{-1} indicated the presence of Zn-O bond (Fig S13 C, D).

The presence of N-H stretch between 3,500-3,100 cm^{-1} in the full scan FTIR spectra could be contributed by the proteins present in the bacterial cells (Fig S13B). These results reconfirmed the presence of zinc ferrite and zinc oxide in the treated bacteria.

While the exact mechanism of the biosynthesis is unclear, it can be construed that on uptake, soluble Fe (II), in presence of oxygen would induce oxidative stress via the Fenton reaction. We evaluated the oxidative stress in the respective microbes using ROS assay. As displayed in Fig 4, treatment with iron *per se* increased the ROS levels. In comparison, the bacteria treated with zinc alone, and in combination with iron, displayed an additional significant increase in the ROS levels. This data reaffirmed the role of zinc in inducing oxidative stress [34]. The results suggested that in comparison to iron, zinc was a more potent inducer of ROS. This data is supported by a recent study in which excess zinc was shown to increase both intracellular iron and oxidative stress in *E. coli* [35]. It is likely that ROS is involved in the biomineralization process, as only those microbes expressing high levels of ROS revealed intracellular iron accumulation and nanoparticle synthesis (Table S1). In an earlier study, we had reported ROS involvement in inducing MNP synthesis in eukaryotic cells treated with a similar combination of Fe and Zn precursors [21].

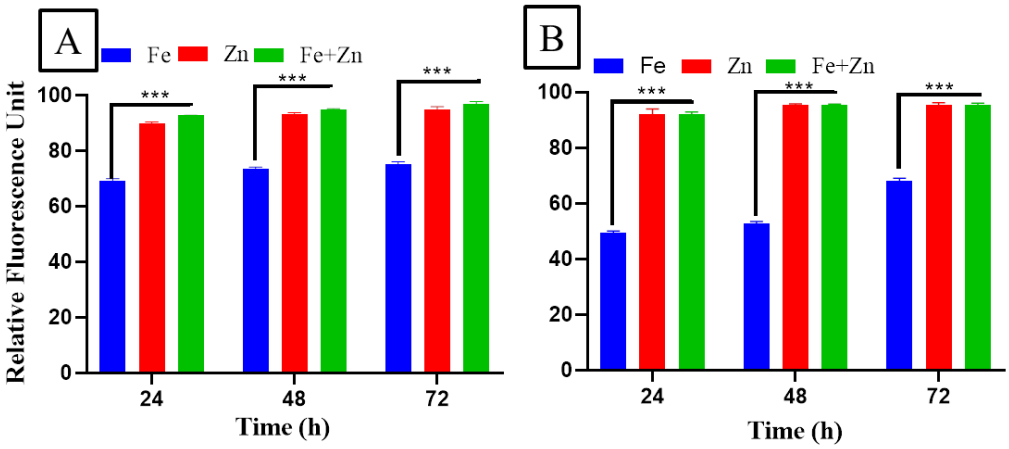

Fig 4: Time dependent ROS expression. (A) *S. aureus* and (B) *E. coli* treated with $FeCl_2$ /zinc gluconate/both for 24-72 h. The data represents the mean ± SD obtained from 3 experiments in which N=3 in each group. Two-way ANOVA Bonferroni multiple comparison test where *** represents p-value <0.001.

Magnetotactic bacteria (MTB) are the only naturally occurring bacteria that can produce intracellular MNP and exhibit magnetotaxis in response to magnetic field [36]. MNP containing magnetosomes-derived from MTB are known to induce magnetic field-dependent temperature rise

on exposure to AMF [37]. Reports indicate that MNP with diameters <15 nm are most effective for generating hyperthermia [38], and that zinc ferrite nanoparticles have better magnetization properties [32]. As the biosynthesized MNP is made of zinc ferrite in the size range of 13-19 nm, we evaluated its heating potential. On exposure of the treated bacteria to AMF at two different frequencies i.e. 164 KHz and 347 KHz for 30 min, the respective bacterial suspension displayed a time dependent increase in temperature, with an improved heating outcome at 347 KHz (Fig 5A). To check the post-AMF viability, the bacterial suspension before and after respective AMF treatment was spread on agar plates and the colonies checked after 24 h (Fig 5B). A dramatic decrease in the number of bacterial colonies obtained after exposure to AMF implied the susceptibility of bacteria to hyperthermia (Fig. 5 C&D). The significant temperature rise observed with the higher frequency, translated to an increase in cell death as compared to lower frequency. Field emission-scanning electron microscopic images revealed the distorted morphology of the bacteria post-AMF (Fig 5Eb).

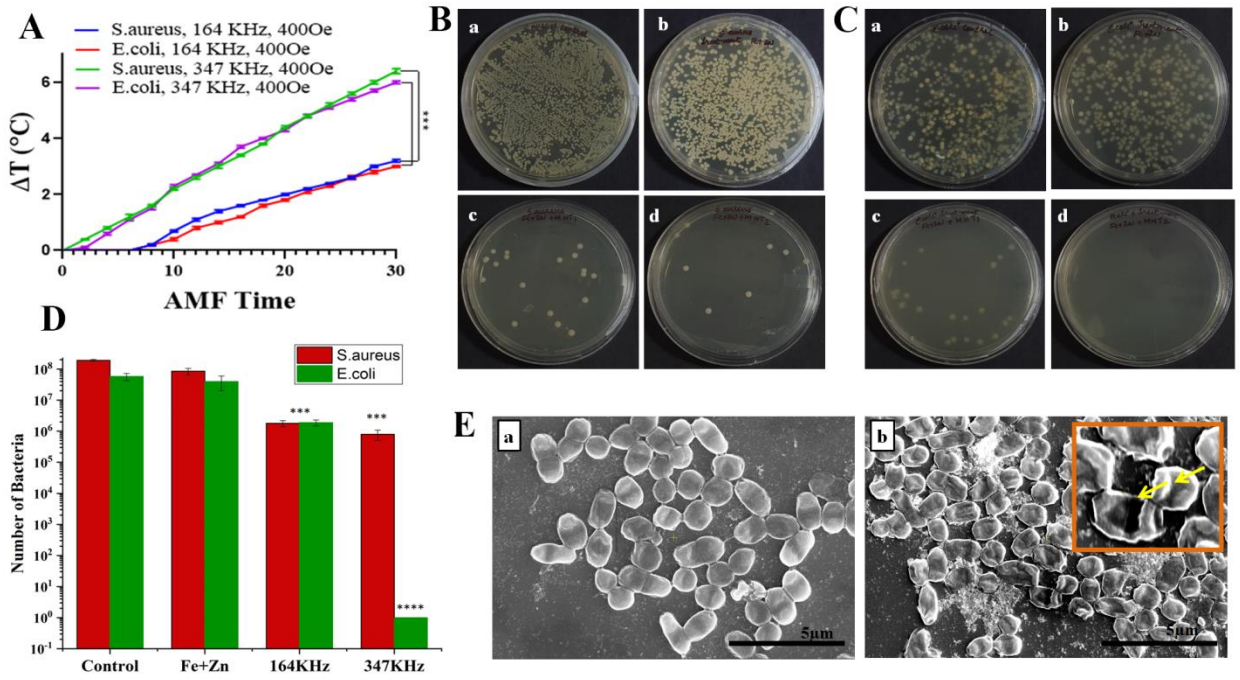

Fig 5: Bacterial response to hyperthermia (A) Time and magnetic-field -dependent temperature change in *S. aureus* and *E.coli*. Bacterial cell colonies obtained post-AMF of (B) *S. aureus* and (C) *E. coli*, wherein, (a) represents untreated bacteria (b) bacteria treated with $FeCl_2$ and zinc gluconate (c) Treated bacteria exposed to AMF at164 KHz, 400Oe and (d) Treated bacteria exposed to AMF at 347 KHz, 400Oe; (D) Number of bacterial colonies obtained after AMF treatment in *S. aureus* and *E .coli*, where

the data represents the mean ± SD obtained from 3 experiments in which N=3 in each group. Two-way ANOVA Bonferroni multiple comparison test where *** represents p-value <0.001 and **** represents p-value<0.0001. (E) FE-SEM images of treated bacteria (a) before and (b) after AMF.

Biofilms are resistant to antibiotics and protective immune responses due to the impervious protective material lay down by the surface adhered bacteria [39]. To check if the bacteria in the biofilms are capable of MNP synthesis and susceptible to hyperthermia, the biofilms prepared with *S. aureus* (Fig 6A) and *E. coli* (Fig 6B) were treated with Fe and Zn precursors for 36 h. The treated biofilms were exposed to AMF for 30 min and the bacterial viability was evaluated using live/dead staining. A remarkable decrease in the number of viable cells, suggested that Fe and Zn had penetrated the biofilms and induced bacterial MNP synthesis. The MNP in presence of a magnetic field induced heating, leading to bacterial cell death.

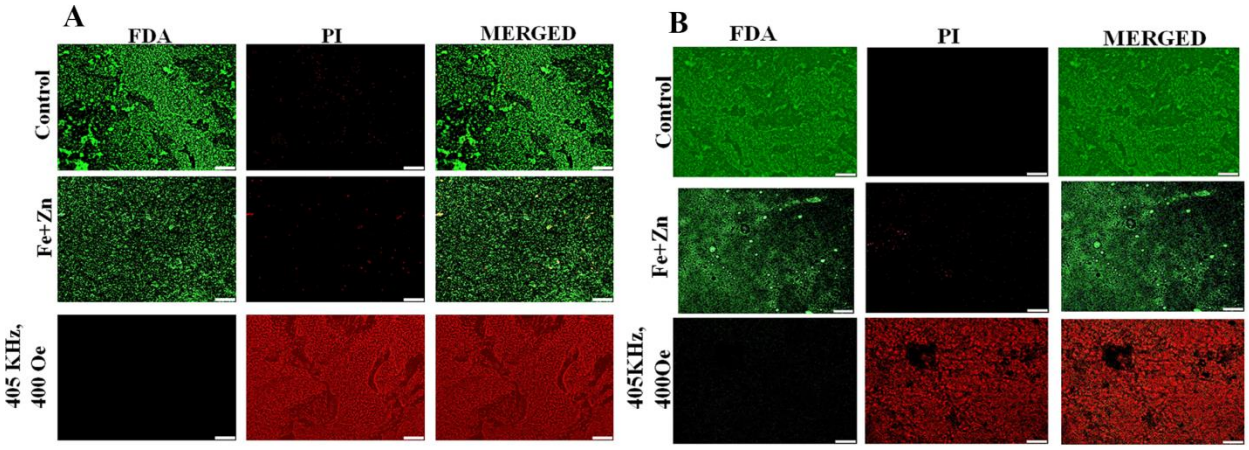

Fig 6: Hyperthermia response in biofilms treated with $FeCl_2$ and Zn gluconate. Visualization of live (green)/dead (red) using fluorescence microscope. (A) *S. aureus* (B) *E. coli b*iofilms treated with FDA/PI after AMF exposure.

As pathogenic bacteria overcome the host's nutritional immunity and gain access to elements like iron and zinc, their uptake in bacteria is regulated by the metal-dependent Fur/Zur family of proteins which control the respective genes involved in their acquisition. Apart from normal physiological processes, these regulatory proteins are also responsible for the expression of virulence factors [40]. Apart from the known mechanisms of Fe and Zn regulation, we assessed if the acquired elements are also converted to MNP. Multiple infected human specimens

represented in Table S2 were tested after receiving the ethics committee approval from PGIMER, Chandigarh. The pathogenic bacteria in each specimen were identified by Gram-staining and the samples were stained with Perl's Prussian blue. A blue color in the bacteria denoted the presence of iron oxide. To confirm the presence of MNP in these bacteria, the infected plasma samples were evaluated using TEM. TEM images of *E.coli* infected plasma revealed the presence of several nanocrystals randomly distributed in the bacteria (Fig 7A). Analysis of the carbonized bacteria, displayed ~ 20 nm spherical, crystalline nanoparticles of iron oxide (Fig 7Aa). To determine the hyperthermia response, the infected blood samples were depleted of RBC, and the resulting plasma was exposed to AMF at 347 KHz, 400 Oe for 30 min. A time-dependent increase in temperature was noted in all samples, with the response being dependent on the type of bacteria (Fig 7B). The bacterial growth evaluated post-AMF exposure, showed a drastic reduction in colonies (Fig 7 C, D).

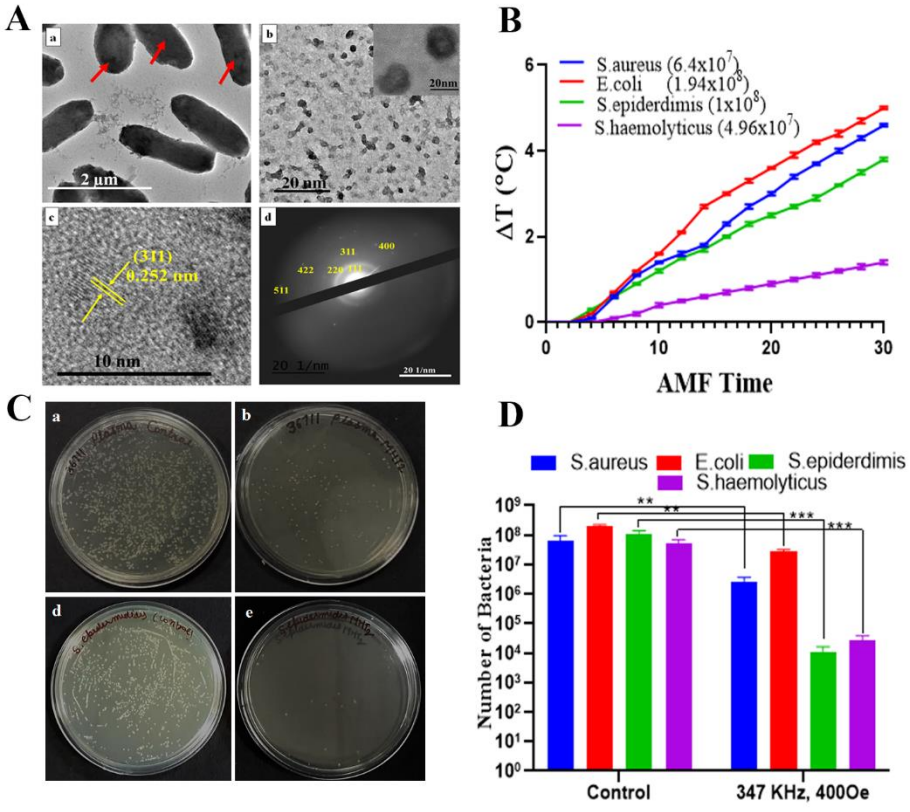

Fig 7: **Blood plasma Characterization and response to hyperthermia:** (A) TEM images of *E.coli.* (a) *E.coli* infected blood (arrow indicates nanoparticles); (b) Nanoparticles obtained from carbonized *E.coli* sample (inset indicates nanoparticles); (c,) HR-TEM showing D-Planar spacing of nanoparticles; (d) SAED

pattern of nanoparticles. (B) Time and magnetic-field -dependent temperature change in *S. aureus*, *E. coli*, *S. epiderdimis*, *S. haemolyticus.* The total number of respective bacteria is mentioned in brackets. (C) Bacterial cell colonies obtained post-AMF where, upper panel shows *S. aureus* and lower panel is *S. epiderdimis*, wherein, (a,c) represents untreated bacteria (b, d) bacteria exposed to AMF at 347 KHz, 400 Oe; (D) Number of bacterial colonies obtained after AMF treatment in *S. aureus, E. coli, S. epiderdimis, S. haemolyticus*. The data represents the mean ± SD obtained from 3 experiments in which N=3 in each group. Two-way ANOVA Bonferroni multiple comparison test where ** represents p-value <0.01 and *** represents p-value<0.001.

To determine the efficacy of hyperthermia-induced bacterial cell death in infected tissues, *E. coli* infected dermal and bone samples were exposed directly to AMF at 347 KHz, 400 Oe. The respective tissues, pre-and post-AMF were homogenized and the bacterial growth assessed in the homogenates (Fig.S14 C&D). A considerable reduction in bacterial load post-AMF showed the potential of magnetic-hyperthermia- induced treatment to control bacterial infections.

Conclusion

In conclusion, we report the inherent ability of pathogenic bacteria to form intracellular MNP in presence of essential elements like iron and zinc. The MNP endow the bacteria with magnetic-field induced motility, a property that can be used for bacterial separation. On exposure to AMF, the MNP response leads to a temperature rise, resulting in bacterial susceptibility. Exposure of biofilms to these elements, and its subsequent exposure to AMF, resulted in a similar dramatic reduction in bacterial viability, suggesting the potential of this approach to address biofilms. Finally, identification of MNP in bacteria derived from infected tissues established the phenomenon of intracellular MNP formation. The susceptibility of such bacteria to magnetic field-induced hyperthermia, suggested that infectious bacteria can be directly destroyed by AMF. This strategy provides a hitherto unknown approach to combat infectious bacteria.

Author contributions

SK: Investigated, Visualized and compiled the manuscript. JT, RS, HSR and VC: Investigated and visualized the data. VP: Analyzed the data; RK: Supported with microbial cultures; VG provided essential microbial strains, supported the investigations and edited the manuscript. DG: Conceptualized, supervised, secured funding and edited the manuscript. All authors read and approved the final manuscript.

Competing interests Authors declare no competing financial interest.

Acknowledgements

We thank Dr. Erik T. J. Nibbering, Max-Born-Institut and Dr. Narayan Pradhan from IACS, Kolkata for reviewing the manuscript. The support of Dr. Chayan K. Nandi (IIT, Mandi) and Dr. Suvankar Chakraverty, INST and Dr. Nitin Singhal, NABI is acknowledged. The authors thank Ms. Gurleen Kaur for assistance with graphics. The authors thank Department of Biotechnology (BT/PR22067/NNT/28/1163/2016), Department of Science and Technology (SERB/F/755/2019-2020), India for partially funding the project.

Appendix A. Supplementary material

Correspondence and requests for materials should be addressed to Deepa Ghosh (deepa.ghosh@inst.ac.in)

References:

1. R.I. Aminov, Front. Microbiol. 1(2010) 1-7. https://doi.org/10.3389/fmicb.2010.00134.
2. https://www.who.int/medicines/areas/rational_use/prioritization-of-pathogens/en, 2017.
3. O.Cars, L.D.Hogberg, M.Murray, O.Nordberg, S.Sivaraman, C.S.Lundborg, A.D. So Goran Tomson. BMJ. 18 (2008) 726-728. https://doi.org/10.1136/bmj.a1438
4. C. Årdal, M. Balasegaram, R. Laxminarayan, D. McAdams, K. Outterson, J. H. Rex, N. Sumpradit, Nat. Rev. Microbiol. 18 (2020) 267-274. https://doi.org/10.1038/s41579-019-0293-3.
5. D. A Six, T. Krucker, J. A. Leeds, Curr .Opin. Chem. Biol. 44 (2018) 9-15. https://doi.org/10.1016/j.cbpa.2018.05.005.
6. L. Gloag, M. Mehdipour, D, Chen, R. D. Tilley, J. J. Gooding, Adv. Mater. 31 (2019) 1-26. https://doi.org/10.1002/adma.201904385.
7. H. Shen, J.Wang, H. Liu, Z. Li, F. Jiang, Fu-Bing Wang, Q. Yuan, ACS Appl. Mater. Interfaces. 8 (2016) 19371–19378. https://doi.org/10.1021/acsami.6b06671
8. J. Wang, X. Wu, C. Wang, Z. Rong, H. Ding, H. Li, S. Li, N. Shao, P. Dong, R. Xiao, S. Wang, ACS Appl. Mater. Interfaces. 8 (2016) 19958–19967. https://doi.org/10.1021/acsami.6b07528
9. J. Wang, H. Wu, Y. Yang, R. Yan, Y. Zhao, Y. Wang, A. Chen, S. Shao, P.Jiang, Yong- Qiang Li , Nanoscale. 10 (2018) 132-141. https://doi.org/10.1039/C7NR06373C .
10. Y. Xu, H. Wang, C. Luan, Y. Liu, B. Chen, Y. Zhao, Biosens. Bioelectron. 100 (2018) 404-410. https:// doi: 10.1016/j.bios.2017.09.032.
11. S. Lefevre, D. Ruimy, F. Jehl, A. Neuville, P. Robert, C. Sordet, M. Ehlinger, Jean-Louis Dietemann, G.Bierry, Radiol. 258 (2011) 722-728. https://doi.org/10.1148/radiol.10101272.

12. K. L.Ribeiro, I.A.M.Frías, O. L.Franco, S. C.Dias, A. A.Sousa-Junior, O. N.Silva, A. F.Bakuzis, M. D.L.Oliveira, C. A.S.Andrade, Colloids Surf. B. 169 (2018) 72-81. https://doi.org/10.1016/j.colsurfb.2018.04.055

13. X. Wang, A. Deng, W. Cao, Q. Li, L. Wang, J. Zhou, B. Hu, X. Xing, J. Mater. Sci. 53 (2018) 6433–6449(2018). https://doi.org/10.1007/s10853-018-1998-9.

14. L. de Alcântara S. de Toledo, H. C. Rosseto, M. L. Brusch, Pharm. Dev. Technol. 23 (2018) 316-323. https://doi.org/10.1080/10837450.2017.1337793

15. C.Xu, Ozioma Udochukwu Akakuru, Jianjun Zheng, Aiguo Wu, Front. Bioeng. Biotechnol. 7 (2019) 1-15. https://doi.org/10.3389/fbioe.2019.00141

16. G. Oberdorster, E. Oberdorster, J. Oberdorster, Environ Health Perspect. 113 (2005) 823-839. https://doi: 10.1289/ehp.7339.

17. Min-Ho Kim, I. Yamayoshi, S. Mathew, H. Lin, J. Nayfach, S. I. Simon, Ann Biomed Eng. 41 (2013) 598–609. https://doi.org/10.1007/s10439-012-0698-x.

18. S.K.Sharma, N. Shrivastava, F. Rossi, Le DucTung, N. T. K..Thanh, Nanotoday. 29 (2019) 598–609. https://doi.org/10.1016/j.nantod.2019.100795

19. G. R. Rodrigues, C. López-Abarrategui, I. la S. Gomez, S. C. Dias, A. J.Otero-González, O. L. Franco, Int. J. Pharm. 555 (2019) 356-367. https://doi.org/10.1016/j.ijpharm.2018.11.043

20. Rui-ting Liu, J. Liu, Jie-qiongTong, T.Tang, Wei-ChaoKong, Xiao-wen Wang, Y. Li, Prog. Nat. Sci. 22 (2012) 31-39. https://doi.org/10.1016/j.pnsc.2011.12.006.

21. S. Kaushik, J. Thomas, V.Panwar, H. Ali, V. Chopra, A. Sharma, R. Tomar, D. Ghosh, ACS Appl. Bio Mater. 3 (2020) 779–788. https://doi.org/10.1021/acsabm.9b00720

22. M. I. Hood, E. P. Skaar, Nat. Rev. Microbiol. 16 (2012) 525-537. https://doi.org 10.1038/nrmicro2836

23. Li Ma., A. Terwilliger, A. W. Maresso, Metallomics. 7 (2015) 1541-1554. https://doi.org/10.1039/C5MT00170F

24. Z. Xu, P. Wang, H. Wang, Z.H. Yu, H. Y. A. Yeung, T. Hirayama, H. Sun, A.Yan, J. Biol. Chem. 294 (2019) 16978-16991. https://doi.org/10.1074/jbc.ra119.010023.

25. S. C. Andrews, A. K. Robinson, F. Rodríguez-Quiñones, FEMS Microbiology Reviews, 27 (2003) 215–237. https://doi.org/10.1016/S0168-6445(03)00055-X.

26. G.Y.Zhang, Y.Q. Sun, D.Z. Gao, Y.Y. Xu. Mater. Res. Bull. 45 (2010) 755-760. https://doi.org/10.1016/j.materresbull.2010.03.025

27. S.K.Sahoo,G.Hota, ACS Appl. Nano Mater. 2 (2019) 983–996. https://doi.org/10.1021/acsanm.8b02286

28. H. Chen, W. Liu, Z.Q, Catal. Sci. Technol. 7 (2017) 2236-2244. https://doi.org/10.1039/C7CY00308K

29. C. Yao, Q. Zeng, G. F. Goya, T. Torres, J. Liu, H. Wu, M. Ge, Y. Zeng, Y.Wang, J. Z. Jiang,. *J. Phys. Chem. C.* 111 (2007) 12274–12278. https://doi.org/10.1021/jp0732763.

30. T. Hyeon, Chem. Commun. 8 (2003) 927-934. https://doi.org/10.1039/B207789B

31. M. Mazur, A. Barras, V. Kuncser, A. Galatanu, V. Zaitzev, K.V. Turcheniuk, P. Woisel, J. Lyskawa, W. Laure, A. Siriwardena, R. Boukherroub, S. Szunerits, Nanoscale. 7 (2013) 2535 -3084. https://doi.org/10.1039/C3NR33506B

32. J.M. Byrne, V. S. Coker, E. Cespedes, P.L. Wincott, D. J. Vaughan, R.A.D. Pattrick, G. van der Laan, E. Arenholz, F. Tuna, M. Bencsik, J.R. Lloyd, N. D. Telling, Adv. Funct. Mater. 24 (2014) 2518-2529. https://doi.org/10.1002/adfm.201303230

33. X. Wang, L. Huang, Y. Zhao, Y. Zhang, G. Zhou, NRL. 11 (2016) 1-6. https://doi.org/10.1186/s11671-016-1244-9

34. B. A. Eijkelkamp, J.R. Morey, M. P. Ween, Cheryl-lynn Y. Ong, A. G. McEwan, J. C. Paton, C. A. McDevitt , PloS one, 9 (2014) 1-11. https://doi.org/10.1371/journal.pone.0089427.

35. A. Postec, N.Tapia, A. Bernadac, M. Joseph, S.Davidson, L.Fei. Wu, B. Ollivier, N. Pradel, Microb Ecol. 63 (2012) 1-11. https://doi.org/10.1007/s00248-011-9910-z.

36. C. T. Lefèvre, D.A. Bazylinsk, Microbiol Mol Biol Rev. 77(2013) 497–526. https://doi.org/ 10.1128/MMBR.00021-13.

37. E. Alphandery, S. Faure, L. Raison, E. Duguet, P. A. Howse, D. A. Bazylinski, J. Phys. Chem. C. 115 (2011) 18–22. https://doi.org/10.1021/jp104580t.

38. M. Gonzales-Weimuller, M. Zeisberger , K.M. Krishnan, J. Magn. Magn. Mater. 321 (2009) 1947-1950. https://doi.org/10.1016/j.jmmm.2008.12.017

39. C. Bordi, S. de Bentzmann, Ann. Intensive Care. 1(2011) 1-8. https://doi.org/10.1186/2110-5820-1-19.

40. D. Lucarelli , S. Russo, E. Garman, A. Milano, W.Meyer-Klaucke, E.Pohl, J. Biol. Chem. 282,(2007) 9914 –9922.07. https://doi.org/10.1074/jbc.M609974200